BIOCHEMICAL PHARMACOLOGY 77 (2009) 1125–1138

available at www.sciencedirect.com

ScienceDirect

journal homepage: www.elsevier.com/locate/biochempharm

The experimental chemotherapeutic N^6-furfuryladenosine (kinetin-riboside) induces rapid ATP depletion, genotoxic stress, and CDKN1A (p21) upregulation in human cancer cell lines

Christopher M. Cabello, Warner B. Bair III, Stephanie Ley, Sarah D. Lamore, Sara Azimian, Georg T. Wondrak *

Department of Pharmacology and Toxicology, College of Pharmacy, Arizona Cancer Center, University of Arizona, 1515 North Campbell Avenue, Tucson, AZ 85724, USA

ARTICLE INFO

Article history:
Received 14 October 2008
Accepted 3 December 2008

Keywords:
Kinetin
N^6-furfuryladenosine
Genotoxic stress
ATP depletion
CDKN1A
Cancer

ABSTRACT

Cytokinins and cytokinin nucleosides are purine derivatives with potential anticancer activity. N^6-furfuryladenosine (FAdo, kinetin-riboside) displays anti-proliferative and apoptogenic activity against various human cancer cell lines, and FAdo has recently been shown to suppress tumor growth in murine xenograft models of human leukemia and melanoma. In this study, FAdo-induced genotoxicity, stress response gene expression, and cellular ATP depletion were examined as early molecular consequences of FAdo exposure in MiaPaCa-2 pancreas carcinoma, A375 melanoma, and other human cancer cell lines. FAdo, but not adenosine or N^6-furfuryladenine (FA), displayed potent anti-proliferative activity that was also observed in human primary fibroblasts and keratinocytes. Remarkably, massive ATP depletion and induction of genotoxic stress as assessed by the alkaline comet assay occurred within 60–180 min of exposure to low micromolar concentrations of FAdo. This was followed by rapid upregulation of CDKN1A and other DNA damage/stress response genes (HMOX1, DDIT3, and GADD45A) as revealed by expression array and Western analysis. Pharmacological and siRNA-based genetic inhibition of adenosine kinase (ADK) suppressed FAdo cytotoxicity and also prevented ATP depletion and p21 upregulation suggesting the importance of bioconversion of FAdo into the nucleotide form required for drug action. Taken together our data suggest that early induction of genotoxicity and energy crisis are important causative factors involved in FAdo cytotoxicity.

1. Introduction

Cytokinins and cytokinin nucleosides are purine derivatives with potential anticancer activity [1–3]. Originally discovered as phytohormones that promote cell division, leaf expansion, and callus cell redifferentiation [4], early and recent experimental evidence suggests that naturally occurring and synthetic cytokinins target human cancer

* *Corresponding author*. Tel.: +1 520 626 9017; fax: +1 520 626 8567.
E-mail address: wondrak@pharmacy.arizona.edu (G.T. Wondrak).

Abbreviations: 5′-AdA, 5′-amino-5′-deoxyadenosine; ADK, adenosine kinase; Ado, adenosine; AV, annexinV; CDKN1A, cyclin-dependent kinase inhibitor 1A; DDIT3, DNA-damage-inducible transcript 3; FA, N^6-furfuryladenine; FAdo, N^6-furfuryladenosine; FITC, fluorescein isothiocyanate; GADD45A, growth arrest and DNA-damage-inducible, alpha; HMOX1, heme oxygenase 1; PI, propidium iodide; SDS-PAGE, sodium dodecylsulfate polyacrylamide gel electrophoresis.

0006-2952/$ – see front matter
doi:10.1016/j.bcp.2008.12.002

cells through anti-proliferative, apoptogenic, and differentiation-inducing activities [2,3,5,6]. N^6-furfuryladenine(FA, kinetin) is a cytokinin that forms during thermal processing of DNA through water elimination and rearrangement of nucleic acid-bound 2-deoxyribose leading to N^6-alkylation of adenine by furfurylalcohol [7,8]. Together with biosynthetic cytokinins including zeatin and N^6-isopentenyladenine, FA acts as a weak ATP-site directed inhibitor of the cyclin-dependent kinase $p34^{cdc2}$/cyclin B kinase [1]. Pleiotropic pharmacodynamic effects of FA on mammalian cells have been described including antioxidant protection [9], stimulation of proliferation and suppression of oxidative stress-induced senescence in cultured skin fibroblasts [10], and induction of redifferentiation in human leukemia cells [3]. Moreover, rescue of a human mRNA splicing defect by FA-modulation of IKBKAP pre-mRNA processing in familial dysautonomia has been described recently [11].

Importantly, the FA-nucleoside N^6-furfuryladenosine (FAdo, kinetin-riboside) is devoid of cyclin-dependent kinase inhibitory activity [1], but displays potent anti-proliferative activity against various human cancer cell lines, and FAdo together with other cytokinin ribosides including N^6-isopentenyladenosine and N^6-benzyladenosine has recently been shown to suppress proliferation and induce apoptosis in human myeloid leukemia cells [3,6,12–14]. Preclinical antimyeloma activity of FAdo has been demonstrated in a mouse xenograft model of the disease and mechanistically linked to FAdo-mediated inhibition of CCND2 transactivation resulting in down-regulation of cyclin D1 and D2 protein expression involved in cell cycle arrest and apoptosis [14]. Earlier research has demonstrated that FAdo anti-proliferative and apoptogenic activities are antagonized by pharmacological inhibitors of adenosine kinase (ADK), suggesting that FAdo bioactivation through metabolic conversion into the nucleotide form is essential for FAdo cytotoxicity [3,6].

In the current study, we tested the hypothesis that the cytotoxic effects of this adenosine-derivative and nucleotide precursor may involve interference with DNA integrity and cellular energy status leading to stress response gene expression and cell cycle arrest. Our results obtained from MiaPaCa-2 pancreas carcinoma, A375 melanoma, and various other human cancer cell lines indicate that massive ATP depletion and induction of genotoxic stress occurs rapidly in response to FAdo exposure followed by early upregulation of HMOX1, CDKN1A, and other DNA damage/stress response genes. These data suggest that early induction of genotoxicity and energy crisis are causative factors involved in FAdo cytotoxicity and anticancer activity.

2. Materials and methods

2.1. Materials

All chemicals were from Sigma Chemical Co. (St. Louis, MO, USA). The cell-permeable pan-caspase inhibitor Z-VAD-(OMe)-fmk and the cell-permeable caspase 8 inhibitor (AcAA-VALLPAVLLALLAPIETD-CHO) were from Calbiochem–Novabiochem (San Diego, CA, USA).

2.2. General cell culture

G-361 human melanoma cells from ATCC (Manassas, VA, USA) were cultured in McCoy's 5a medium containing 10% bovine calf serum (BCS). Human A375 and LOX metastatic melanoma cells (from ATCC) were cultured in RPMI medium containing 10% BCS and 2 mM L-glutamine. Human HT29 and HCT116 colon carcinoma cells (from ATCC) were cultured in RPMI containing 10% BCS. Human dermal neonatal foreskin Hs27 fibroblasts and MiaPaCa-2 pancreas carcinoma cells (from ATCC) were cultured in DMEM containing 10% fetal bovine serum. Primary human epidermal keratinocytes (neonatal HEKn-APF, from Cascade Biologics, Portland, OR, USA) were cultured using Epilife medium supplemented with EDGS growth supplement and passaged using recombinant trypsin/EDTA and defined trypsin inhibitor. Cells were maintained at 37 °C in 5% CO_2, 95% air in a humidified incubator.

2.3. Cell proliferation assay

Cells were seeded at 10,000 cells/dish on 35-mm dishes. After 24 h, cells were treated with test compound. 5′-Amino-5′-deoxyadenosine (5′-AdA) was added 1 h before exposure to FAdo. Cell number at the time of compound addition and 72 h later were determined using a Z2 Analyzer (Beckman Coulter, Inc., Fullerton, CA, USA). Proliferation was compared with cells that received mock treatment. The same methodology was used to establish IC_{50} values (drug concentration that induces 50% inhibition of proliferation of treated cells within 72 h exposure ± S.D., $n = 3$) of anti-proliferative potency.

2.4. Cell cycle analysis

Cells were seeded at 4×10^5 per T-75 flask (Sarstedt, USA) and left overnight to attach. The next day, cells received treatment with test agents and solvent controls. At 72 h after drug administration, cells were harvested by trypsinization, resuspended in 200 μl PBS, and placed on ice and processed as published recently [18]. After addition of 2 ml 70% (v/v) ethanol, 30% (v/v) PBS, cells were incubated for 30 min on ice. The fixed cells were pelleted by centrifugation, resuspended in 800 μl PBS, 100 μl ribonuclease A (1 mg/ml PBS), and 100 μl propidium iodide (PI, 400 μg/ml PBS), and incubated for 30 min in the dark at 37 °C. Cellular DNA content was determined by flow cytometry and analyzed using the ModFit LT software, Version 3.0 (Verity, Topsham, ME, USA).

2.5. Phospho-histone H3(Ser10) flow cytometry

Human MiaPaCa-2 cells (500,000) were exposed to FAdo (10 μM, 72 h) or left untreated. Cells in M-phase were then detected by bivariate flow cytometric determination of cellular DNA content (PI-staining) and histone H3 phosphorylated at Ser 10 [p-H3(Ser10)] using a rabbit-derived Alexa-488 conjugated antibody (Cell Signaling, Inc., Danvers, MA, USA) according to the manufacture's protocol. p-H3(Ser10)-positive cells in M-phase were expressed in percent of total gated cells (mean ± S.D., $n = 3$).

2.6. Apoptosis analysis

Viability and induction of cell death (early and late apoptosis/necrosis) were examined by annexinV-FITC/propidium iodide (PI) dual staining of cells followed by flow cytometric analysis as published previously [19,20]. Cells (100,000) were seeded on 35 mm dishes and received drug treatment 24 h later. Cells were harvested at various time points after treatment and cell staining was performed using an apoptosis detection kit according to the manufacturer's specifications (APO-AF, Sigma, St. Louis, MO, USA).

2.7. Caspase-3 activation assay

Treatment-induced caspase-3 activation was examined in MiaPaCa-2 cells using a cleaved/activated caspase-3 (asp 175) antibody (Alexa Fluor 488 conjugate, Cell Signaling, Inc., Danvers, USA) followed by flow cytometric analysis as published recently [20]. Briefly, cells were harvested at various time points after treatment, resuspended in PBS and fixed in 1% formaldehyde. Cells were then permeabilized using 90% methanol and resuspended in incubation buffer (PBS, 0.5% BSA). After rinsing by centrifugation, cells were resuspended in incubation buffer (90 μl) and cleaved caspase-3 antibody (10 μl) was added. After incubation (40 min) followed by rinsing and centrifugation in incubation buffer, cells were resuspended in PBS and analyzed by flow cytometry.

2.8. Cell Glo ATP assay

Cells were seeded at 50,000 cells/dish on 35-mm dishes. After 24 h, cells were treated with test compound. At various time points cells were counted, and ATP content per 10,000 cells was determined using the CellTiter-Glo luminescent assay (Promega, Madison, WI, USA) according to the manufacturer's instructions. Data are normalized to ATP content in untreated cells and expressed as means ± S.D. ($n = 3$).

2.9. Comet assay (alkaline single cell electrophoresis)

The alkaline comet assay was performed on A375 and MiaPaCa-2 cells according to the manufacturer's instructions (Trevigen, Gaithersburg, MD, USA) as published recently [21]. Cells were seeded at 100,000 per 100 mm dish 24 h prior to treatment. Untreated cells were used as a negative control group. After treatment, cells were harvested by gently scraping, rinsed with ice-cold DPBS and suspended in 500 μl DPBS. 50 μl the cell suspension was mixed with 450 μl low-melting-point agarose and spread on pretreated microscope slides. Slides were allowed to dry protected from light, then immersed in ice cold lysis solution plus 10% DMSO and incubated at 4 °C for 45 min. To allow DNA unwinding and expression of alkali-labile sites, slides were exposed to alkaline buffer (1 mmol/l EDTA and 300 mmol/l NaOH, pH > 13) protected from light at room temperature for 45 min. Electrophoresis was conducted in the same alkaline buffer for 20 min at 300 mA. After electrophoresis, slides were rinsed three times in ddH_2O then fixed in 70% ethanol for 5 min. Slides were dried for at least 1 h at 32 °C. Cells were then stained with SYBR® Green and analyzed with a fluorescence microscope (fluorescein filter) and analyzed using CASP software. Up to 75 tail moments for each group were analyzed in order to calculate the mean ± S.D. for each group.

2.10. Phospho-H2A.X detection by flow cytometry

Treatment-induced accumulation of nuclear phosphorylated histone variant H2A.X (γ-H2AX) was examined in MiaPaCa-2 cells using a phospho-histone H2A.X (Ser139) monoclonal antibody (Alexa Fluor 488 conjugate, Cell Signaling, Inc., Danvers, MA, USA) followed by flow cytometric analysis. Cells were harvested at various time points after treatment and processed for flow cytometry as specified above for analysis of procaspase-3 cleavage.

2.11. Human Stress and Toxicity PathwayFinder™ RT² Profiler™ PCR Expression Array

After pharmacological exposure, total cellular RNA (3×10^6 MiaPaCa-2 cells) was prepared using the RNeasy kit (Qiagen, Valencia, CA, USA) according to the manufacturer's instructions. Reverse transcription was performed using the RT² First Strand kit (SA Biosciences, Frederick, MD, USA) and 5 μg total RNA. The Human Stress and Toxicity PathwayFinder™ RT² Profiler™ PCR Expression Array (SuperArray, Frederick, MD, USA) profiling the expression of 84 stress- and toxicity-related genes was run using the following PCR conditions: 95 °C for 10 min, followed by 40 cycles of 95 °C for 15 s alternating with 60 °C for 1 min (Applied Biosystems 7000 SDS, Foster City, CA, USA). Gene-specific product was normalized to GAPDH and quantified using the comparative ($\Delta\Delta C_t$) Ct method as described in the ABI Prism 7000 sequence detection system user guide. Expression values were averaged across three independent array experiments, and standard deviation was calculated for graphing.

2.12. HMOX1, CDKN1A, DDIT3, GADD45A, and ADK expression analysis by real time RT-PCR

Total cellular RNA (3×10^6 cells) was prepared according to a standard procedure using the RNEasy kit from Qiagen (Valencia, CA, USA). Reverse transcription was performed using TaqMan Reverse Transcription Reagents (Roche Molecular Systems, Branchburg, NJ, USA) and 200 ng of total RNA in a 50 μl reaction. Reverse transcription was primed with random hexamers and incubated at 25 °C for 10 min followed by 48 °C for 30 min, 95 °C for 5 min, and a chill at 4 °C. Each PCR reaction consisted of 3.75 μl of cDNA added to 12.5 μl of TaqMan Universal PCR Master Mix (Roche Molecular Systems), 1.25 μl of gene-specific primer/probe mix (Assays-by-Design; Applied Biosystems, Foster City, CA, USA) and 7.5 μl of PCR water. PCR conditions were 95 °C for 10 min, followed by 40 cycles of 95 °C for 15 s, alternating with 60 °C for 1 min using an Applied Biosystems 7000 SDS and Applied Biosystems' Assay-On-Demand primers specific to CDKN1A (p21, assay ID Hs00355782_m1), HMOX1 (heme oxygenase-1, assay ID Hs00157965_m1), DDIT3 (DNA-damage-inducible transcript 3, assay ID Hs00358796_g1), GADD45A (growth arrest and DNA-damage-inducible, alpha, assay ID Hs00169255_m1), and ADK (assay ID Hs00417073_m1). Gene-specific product was normalized to ACTB (β-actin, assay ID Hs99999903_m1; for ADK) or glyceraldehyde-3-phosphate

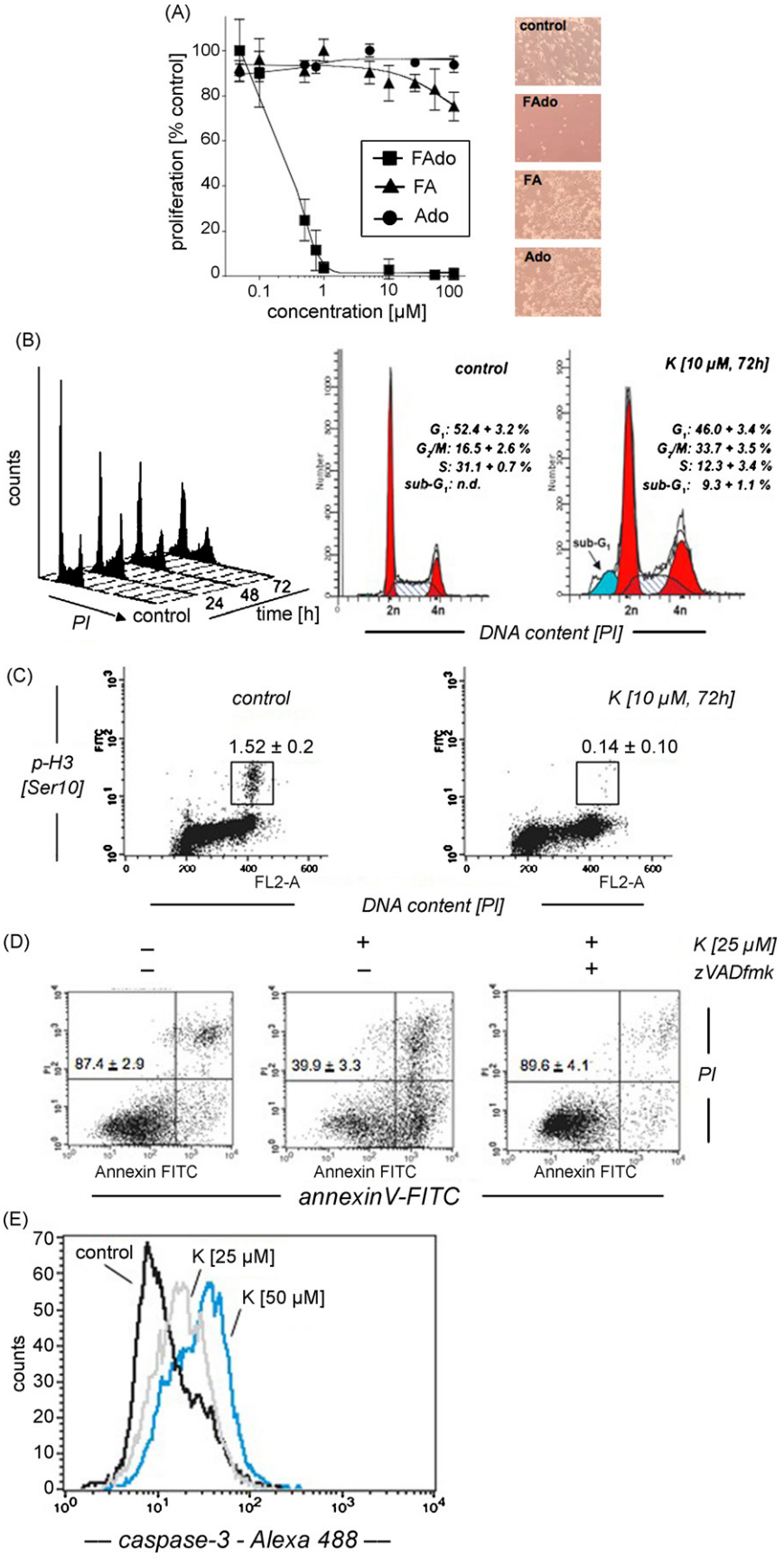

Fig. 1 – Anti-proliferative and apoptogenic activity of FAdo observed in MiaPaCa-2 cells. (A) Dose–response relationship of FAdo-induced inhibition of cell proliferation. After 72 h exposure to increasing concentrations of N^6-furfuryladenosine (FAdo), FA, and adenosine (Ado), proliferation was examined by cell counting and expressed as % of untreated control

dehydrogenase (GAPDH, assay ID Hs99999905_m1; all other genes) and quantified as described above.

2.13. siRNA transfection

A375 cells were transiently transfected with a 100 nM pool of four siRNA oligonucleotides targeting ADK or a 100 nM pool of four non-targeting siRNA oligonucleotides using the DharmaFECT 1 transfection reagent (Dharmacon RNA Technologies, Lafayette, CO, USA). The sequences of siGENOME ADK SMARTpool (ADK siRNA) [GenBank: NM001123] were AGGGAGAGAUGACACUAUA; GGAGAGAUGACACUAUAAU; AAAGUUAUGCCUUAUGUUG; and GAGAGAUGACACUAUAAUG. The oligos were resuspended in the Dharmacon 1× siRNA buffer and incubated in serum-free media for 5 min. DharmaFECT 1 was also incubated in serum-free media for 5 min prior to the addition of the siRNA oligos. The oligos were incubated with the transfection reagent for 20 min prior to cellular treatment. Complete media was added to the siRNA oligo mixture and the cells were incubated with the siRNAs in appropriate cell culture conditions for 72 h. Cells were than re-transfected with another 100 nM pool of four siRNA oligonucleotides targeting ADK or a 100 nM pool of four non-targeting siRNA oligonucleotides. Twenty-four hours after the second transfection, cells were either harvested for expression analysis or plated for proliferation and ATP depletion assays. The relative expressions of the genes of interest were determined using the Relative Expression Software Tool (REST) as previously described [15,16].

2.14. p21 (Waf1/Cip1) immunoblot analysis

One day before treatment, 1×10^6 cells were seeded in a T-75 flask. Medium was replaced 24 h after seeding, followed by addition of test compounds 60 min after medium change. In experiments with 5′-AdA, the compound was added 1 h before addition of FAdo. Cells were incubated for 24 h (37 °C, 5% CO_2), then washed with PBS, lysed in 1× SDS-PAGE sample buffer (200 μl, 0.375 M Tris–HCl pH 6.8, 50% glycerol, 10% SDS, 5% β-mercaptoethanol, 0.25% bromophenol blue), and heated for 3 min at 95 °C prior to separation by 15% SDS-PAGE. Mouse anti-p21 monoclonal antibody (Cell Signaling Technology, Danvers, MA, USA) was used 1:2000 in 5% milk-PBST overnight at 4 °C. The membrane was washed three times for 10 min in 0.1% PBST before adding HRP-conjugated horse anti-mouse antibody (Cell Signaling Technology, Danvers, MA, USA) at 1:2000 dilution. Equal protein loading was examined by α-actin-detection using a mouse anti-actin monoclonal antibody (Sigma, Saint Louis, MO, USA).

2.15. Heme oxygenase-1 (HO-1) immunoblot analysis

Cell extraction, 15% SDS-PAGE, and Western transfer were performed as specified for p21 immunoblot analysis. HO-1 immunodetection was performed as described earlier [17].

2.16. Statistical analysis

Unless indicated differently, the results are presented as means ± S.D. of at least three independent experiments. They were analyzed using the two-sided Student's t-test (*$p < 0.05$; **$p < 0.01$; ***$p < 0.001$).

3. Results

3.1. N^6-furfuryladenosine, but not adenosine or N^6-furfuryladenine, displays anti-proliferative and apoptogenic activity against human MiaPaCa-2 pancreas carcinoma and other cancer cell lines

First, anti-proliferative activity of FAdo was assessed in cultured human MiPaCa-2 pancreas carcinoma cells, where significant inhibition of cell proliferation was observed at submicromolar concentrations (IC_{50}: 0.27 ± 0.09 μM) (Fig. 1A and Table 1). In contrast, no significant anti-proliferative activity of the unsubstituted nucleoside component, adenosine (Ado), and the non-nucleoside base component, N^6-furfuryladenine (FA), was detected. We then examined the effects of prolonged exposure to FAdo (10 μM, 24, 48, and 72 h) on MiaPaCa-2 cell cycle distribution using flow cytometric analysis of PI-stained cells (Fig. 1B). Significant accumulation of cells in G_2/M could be observed starting at 24 h exposure (Fig. 1B, left panel). After 72-h continuous exposure, flow cytometric analysis of PI-stained cells demonstrated depletion of cells in S-phase (by approximately 20% versus untreated controls) and accumulation of cells in G_2/M-phase (by approximately 15% versus untreated controls) (Fig. 1B, middle and right panels). Moreover, bivariate flow cytometric analysis of FAdo-treated cells for DNA content versus expression of phospho-histone H3(Ser10), an established

(mean ± S.D., $n = 3$). Representative light microscopy pictures taken after 72 h exposure are shown. (B) FAdo-induced cell cycle alterations. Cells were exposed to FAdo (10 μM, 24–72 h) or left untreated and then analyzed by PI-staining followed by flow cytometry; left panel: cellular DNA content as a function of exposure time (24–72 h); right panel: cell cycle distribution after 72 h exposure versus untreated control (middle panel) was determined by Modfit data analysis as indicated in Section 2. Numbers indicate means ± S.D., $n = 3$. The arrow indicates dead cells in sub-G_1-phase. (C) FAdo-induced depletion of cells in M-phase. Cells were treated as described for panel B, and expression of phospho-histone H3(Ser10) indicative of cells in M-phase was analyzed by bivariate flow cytometric determination. Numbers indicate p-H3(Ser10)-positive cells in M-phase (squares) in percent of total gated cells (means ± S.D., $n = 3$). (D) Induction of cell death upon extended exposure (48 h) to FAdo (25 μM) in the absence or presence of the pan-caspase inhibitor zVADfmk (42 μM) as assessed by flow cytometric analysis of annexinV-FITC/propidium iodide-stained cells. The numbers indicate viable cells (AV^-, PI^-, lower left quadrant) in percent of total gated cells (mean ± S.D., $n = 3$). (E) FAdo-induced (25 and 50 μM, 48 h) caspase-3 activation was examined by flow cytometric detection using an Alexa Fluor 488-conjugated monoclonal antibody against cleaved procaspase-3. One representative experiment of three similar repeats is shown.

Table 1 – FAdo anti-proliferative activity against primary human skin cells and human melanoma, colon, and pancreas cancer cell lines.

Cell line	IC_{50} (FAdo, μM)
G361	1.52 ± 0.52
LOX	0.16 ± 0.02
A375	0.28 ± 0.01
HT29	3.00 ± 0.65
HCT116	0.72 ± 0.02
MiaPaCa-2	0.27 ± 0.09
HEK	0.11 ± 0.03
Hs27	0.18 ± 0.01

IC_{50} values of FAdo-induced inhibition of proliferation of human skin cells [primary keratinocytes (HEK) and dermal fibroblasts (Hs27)] and melanoma (A375, G361, and LOX), colon (HT29 and HCT116), and pancreas (MiaPaCa-2) cancer cell lines (mean ± S.D., $n = 3$) were determined in proliferation assays as specified in Section 2.

M-phase marker [22], demonstrated that accumulation of cells in G_2/M was accompanied by loss of phospho-H3(Ser10)-positive cells (Fig. 1C). This suggests that FAdo-treatment induces G_2-arrest with complete depletion of cells undergoing mitosis.

Importantly, a significant portion of cells exposed to FAdo (10 μM, 72 h) displayed staining in the sub-G_1 peak of the histogram (approximately 10%) indicative of apoptotic cell death (Fig. 1B, right panel), but cell viability at 24 h exposure time was still fully maintained (Fig. 1B, left panel) as also assessed by trypan blue exclusion and annexinV-PI staining (data not shown). At higher concentrations of FAdo (≥20 μM), prolonged exposure (≥48 h) was associated with massive induction of apoptosis as detected by flow cytometry using annexinV/PI staining (Fig. 1D). FAdo-induced apoptosis was completely blocked in the presence of the pan-caspase inhibitor zVAD-fmk (Fig. 1D), but not in the presence of a caspase 8-selective inhibitor (data not shown) [20]. FAdo-induced proteolytic activation of caspase 3 in MiaPaCa-2 cells occurred dose-dependently (25 and 50 μM FAdo, 48 h exposure) and was demonstrated by flow cytometric analysis using an Alexa488-conjugated antibody that recognizes cleaved procaspase 3 (Fig. 1E).

Anti-proliferative and apoptogenic activity of FAdo was then examined in a panel comprising three human metastatic melanoma (A375, G361, and LOX), two metastatic colon cancer (HT29 and HCT116), and two pancreas carcinoma (MiaPaCa-2 and PANC) cell lines; moreover, FAdo-activity on proliferation of primary human skin keratinocytes and dermal fibroblasts was examined (Table 1). IC_{50} values of FAdo-induced inhibition of proliferation ranged between 0.2 and 6.5 μM for human cancer cell lines cells. When examined in detail in A375 melanoma cells, FAdo-induced cell cycle alterations, and induction of cell death with procaspase 3 cleavage closely resembled the effects observed in MiaPaCa-2 cells (data not shown). Importantly, potent FAdo-anti-proliferative effects ($IC_{50} < 0.2$ μM) were also observed in human primary skin keratinocytes and fibroblasts (Table 1), suggesting a mechanism of anti-proliferative action that does not distinguish between cultured malignant and untransformed primary cells.

Based on these data, it was concluded that (I) FAdo exhibits potent anti-proliferative activity against a broad range of human melanoma, colon, and pancreas cancer cell lines as well as untransformed primary keratinocytes and fibroblasts, (II) FAdo-inhibition of MiPaCa cell proliferation does not occur with close chemical derivatives that represent the incomplete nucleoside, (III) FAdo-inhibition of MiaPaCa-2 and A375 cell proliferation occurs with suppression of DNA synthesis and cell cycle arrest in G2-phase, and (IV) apoptogenicity of high FAdo doses is associated with procaspase 3 cleavage and can be blocked by caspase-inhibition.

3.2. *Pharmacological and genetic antagonism of adenosine kinase suppresses FAdo anti-proliferative and apoptogenic activity*

Earlier experiments using pharmacological inhibitors as molecular probes have provided evidence for the involvement of adenosine kinase in metabolic bioactivation of FAdo in human leukemia cells [3,6,14]. We therefore examined the role of ADK in FAdo anti-proliferative and apoptogenic activity against A375 cells by genetic target modulation using an siRNA approach (Fig. 2A). Knockdown of ADK gene expression was confirmed by real time RT-PCR analysis indicating down-regulation of ADK mRNA by approximately 12.5-fold when compared to control siRNA transfected A375 cells (Fig. 2A, right panel). ADK knockdown in A375 melanoma cells completely blocked the anti-proliferative activity of FAdo (Fig. 2A). Equally, pharmacological inhibition of ADK using the established nucleoside-based ADK-antagonist 5′-amino-5′-deoxyadenosine (5′-AdA) suppressed anti-proliferative (Fig. 2C) activity of FAdo against A375 melanoma cells [23]. Interestingly, siRNA intervention completely protected A375 cells even against high concentrations of FAdo (20 μM), whereas the protective effect of pharmacological ADK inhibition was overcome by high FAdo concentrations that exceeded 5 μM. In MiaPaCa-2 cells, ADK siRNA knockdown was associated with high cytotoxicity, and therefore only pharmacological target modulation using 5′-AdA was performed confirming 5′-AdA antagonism of FAdo anti-proliferative (Fig. 2D) and apoptogenic effects (Fig. 2B). 5′-AdA antagonism of FAdo-induced inhibition of proliferation was also observed in other cell lines contained in our cell panel including Hs27 dermal fibroblasts and G361 metastatic melanoma cells. Our data obtained from pharmacological and genetic target modulation studies demonstrate that FAdo anti-proliferative and apoptogenic activity depends on ADK expression and suggest the involvement of ADK-mediated metabolic conversion of FAdo, presumably into the monophosphate nucleotide.

3.3. *FAdo treatment induces rapid depletion of cellular ATP levels*

Based on earlier work that has demonstrated FAdo-induced ATP depletion in human HL-60 leukemia cells [3,6], we tested the hypothesis that FAdo may interfere with cellular ATP metabolism using a broad panel of cancer cell lines and primary human skin cells. Indeed, using a luciferase-based assay for cellular ATP content dramatic depletion of cellular ATP levels was detected in A375 melanoma (Fig. 3A and B), MiaPaCa-2 (Fig. 3A and C), and other cell lines including G361, LOX, HT29, HCT116, and primary human keratinocytes and dermal fibroblasts (Fig. 3A). The dose–

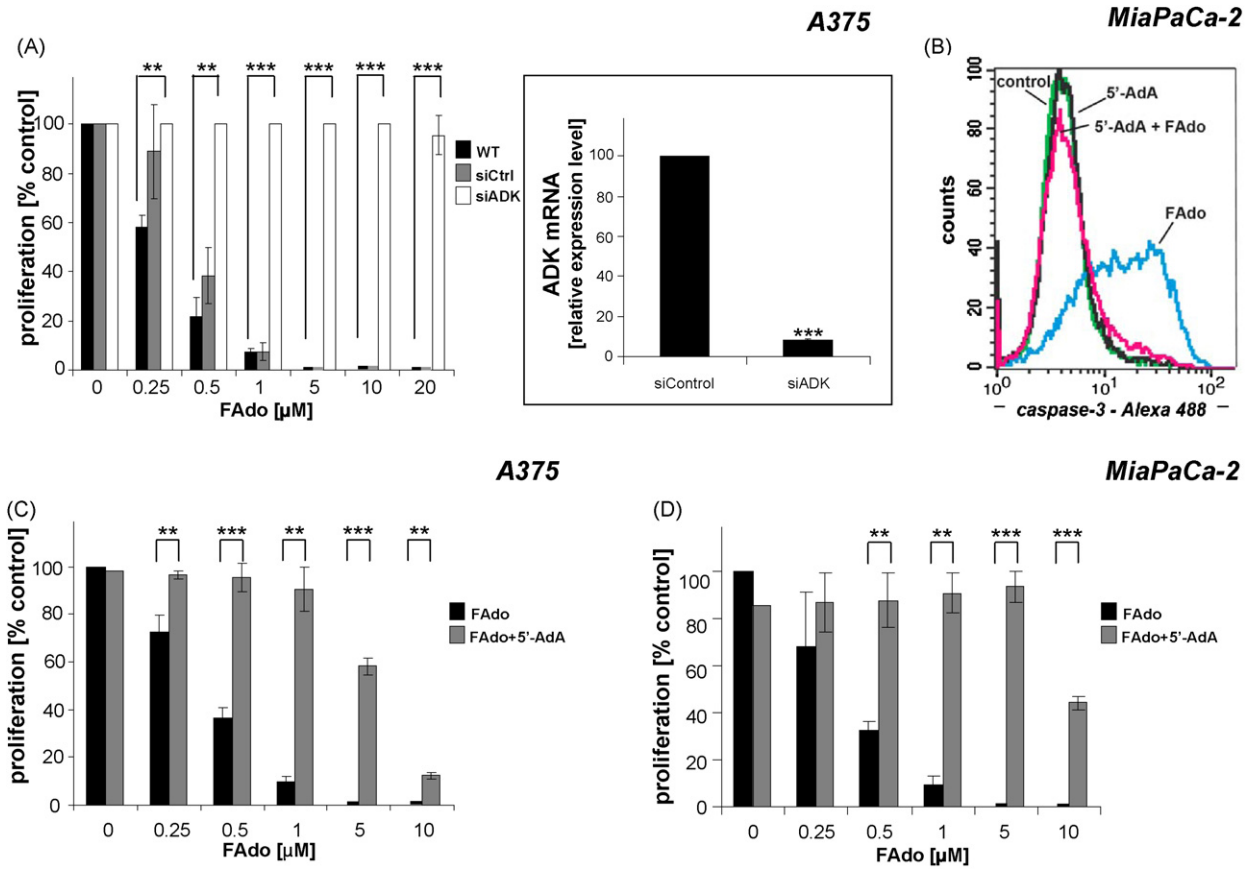

Fig. 2 – Suppression of FAdo anti-proliferative and apoptogenic activity by pharmacological or genetic inhibition of adenosine kinase. (A) Dose–response relationship of FAdo-induced inhibition of A375 cell proliferation in wild type cells (WT) and after control siRNA treatment (siCtrl) and ADK siRNA knockdown (siADK). Knockdown was confirmed by expression analysis using quantitative RT-PCR (right panel; mean ± S.D., $n = 3$) and inhibition of proliferation was assessed as indicated in Section 2. (B) FAdo-induced (50 μM, 48 h exposure) caspase-3 activation in the presence or absence of 5′-AdA (2 μM, added 1 h before FAdo exposure) was analyzed as described in Fig. 1E in MiaPaCa-2 cells. One representative experiment of three similar repeats is shown. Moreover, dose response relationship of FAdo-induced inhibition of A375 (C) and MiaPaCa-2 (D) cell proliferation was tested in the presence or absence of the ADK-inhibitor 5′-AdA (2 μM). After 72 h exposure to FAdo and 5′-AdA, proliferation was examined as described above and expressed as % of untreated control (mean ± S.D., $n = 3$).

effect relationship of FAdo-induced ATP depletion in MiaPaCa-2 and A375 cells suggests that ATP depletion is significant at nucleoside concentrations that exceed 1 μM (Fig. 3B and C). In MiaPaCa-2 cells, cellular ATP levels dropped by over 70% within 24 h exposure to 10 μM FAdo. FAdo-induced ATP depletion in MiaPaCa-2 cells was prevented by coadministration of 5′-AdA (Fig. 3C). Importantly, downregulation of ADK by siRNA or ADK-inhibition by 5′-AdA suppressed FAdo-induced ATP depletion in A375 cells (Fig. 3B), suggesting again that metabolic conversion to the nucleotide form is required for FAdo activation. Interestingly, suppression of ATP depletion by siRNA intervention was more effective than using pharmacological ADK inhibition (5′-AdA), as obvious from the fact that siADK completely prevented ATP depletion even at FAdo concentrations that were able to overcome 5′-AdA-mediated protection (Fig. 3A and B). When the time course of ATP depletion induced by 10 μM FAdo was examined in our cell panel (Fig. 3A), a rapid drop in ATP levels was detectable within 1–3 h of exposure for all cell lines. In MiaPaCa-2 cells, ATP depletion reached a level of statistical significance within 30 min exposure. In these cells, cellular ATP levels were already reduced to approximately 40–60% of untreated controls after 3 h exposure, but did not drop beyond these levels during 12 h exposure (Fig. 3A) or even longer exposure times (Fig. 3C). Importantly, loss of viability or plasma membrane permeabilization measured by trypan blue exclusion and annexinV/PI-staining followed by flow cytometry do not occur over the first 12 h of exposure (data not shown). Taken together these data suggest that rapid and pronounced ATP depletion is an early consequence of FAdo exposure in various cancer cell lines that precedes loss of cell viability and cell cycle arrest and depends on ADK.

3.4. *FAdo treatment rapidly induces cellular genotoxic stress*

Next, we examined the possibility that rapid induction of genotoxic effects may contribute to FAdo-cytotoxicity in MiaPaCa-2 and A375 cells (Fig. 4). Using alkaline single cell

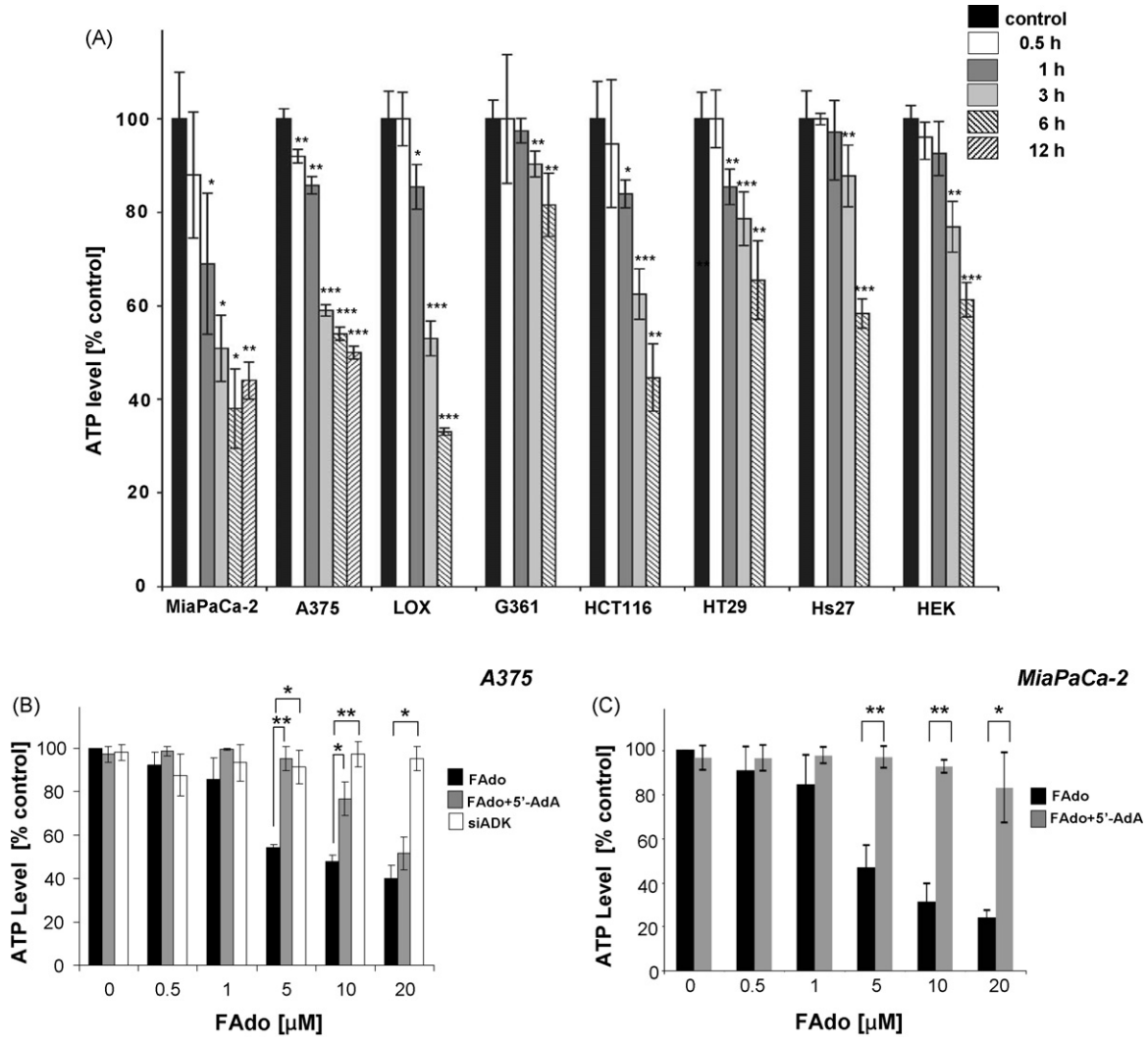

Fig. 3 – Rapid cellular ATP depletion induced by FAdo exposure. Cellular ATP levels were analyzed as a function of FAdo exposure time (panel A) and dose (panels B and C). Data are expressed as % of untreated controls (means ± SD, $n \geq 3$). (A) Time course of ATP depletion in MiaPaCa-2, A375, and other human cancer cell lines and normal primary skin cells (HEK and Hs27) exposed to FAdo (10 μM) for up to 12 h; (B) dose response of ATP depletion in A375 cells (10 μM FAdo, 24 h exposure); additionally ATP levels were assessed if FAdo exposure occurred in the presence of 5′-AdA (2 μM, added 1 h before FAdo exposure) or after ADK siRNA knockdown (siADK) as described in Section 2; (C) ATP depletion in MiaPaCa-2 cells as analyzed in (B).

electrophoresis (comet assay) as a sensitive genotoxicity assay [21,24,25], the integrity of cellular DNA was examined in MiaPaCa-2 and A375 cells treated with FAdo (10 μM, 1–12 h exposure time). As positive controls, cells were exposed to established genotoxic agents including UVB-photons and H_2O_2. Remarkably in both cell lines, 1 h exposure to FAdo was sufficient to induce significant levels of genotoxic stress as evident from formation of nuclear comets (Fig. 4A and B), indicative of DNA unwinding under alkaline conditions resulting from single or double strand breaks, AP-site formation, or nucleotide excision repair [25]. In MiaPaCa-2 cells, the average comet tail moment observed after 1 h exposure exceeded control levels approximately threefold (Fig. 4A). In A375 cells, FAdo treatment induced comets with average tail moments that were increased significantly over untreated controls within 1 h of exposure and exceeded control levels approximately fivefold within 3 h of exposure (Fig. 4B). Overall, the genotoxic effect observed in both cell lines upon FAdo exposure was of only moderate intensity and characterized by very rapid onset. It is important to note that FAdo-induced DNA damage occurs in cells without compromised viability that was maintained over at least 24 h continuous exposure before apoptosis could be detected at 48 h (Fig. 1B, D, and E). In contrast, cells exposed to cytotoxic doses of H_2O_2 or UVB photons serving as positive controls for comet induction displayed a rapid loss of viability with more than 80% cells in apoptosis within 24 h after treatment (data not shown). In an attempt to further characterize the nature of FAdo-induced genotoxicity in MiaPaCa-2 cells, we used flow cytometric detection of the nuclear phosphorylated histone variant H2AX (γ-H2AX, Ser 139), a sensitive marker of DNA double strand breaks and UVB-induced nucleotide excision

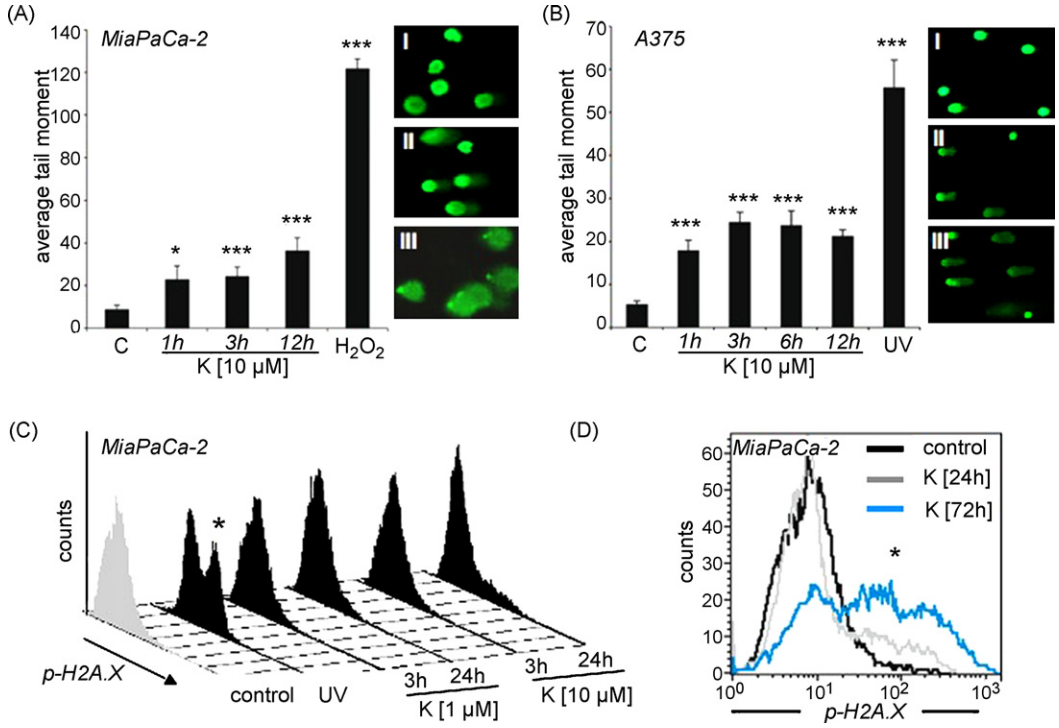

Fig. 4 – Rapid induction of genotoxic stress in human MiaPaCa-2 and A375 cells exposed to FAdo. Cells were exposed to FAdo (1 and 10 μM, 1–24 h) and DNA damage was detected using the comet assay (panels A and B) and flow cytometric detection of phospho-histone H2A.X (Ser139, panels C and D) as described in Section 2. (A) Tail moments observed in MiaPaCa-2 cells. (B) Tail moments observed in A375 cells. As a positive control cells were exposed to H_2O_2 (panel A, 100 μM, 30 min) or UVB (panel B, 240 mJ/cm^2, 3 h postirradiation incubation). Side panels I-III depict comets as visualized by fluorescence microscopy: I. untreated control; II. FAdo-treated (10 μM, 3 h); III. positive control treated as indicated above. (C) Induction of phospho-histone H2A.X in FAdo-treated MiaPaCa-2 cells (UVB control: 240 mJ/cm^2, 3 h postirradiation incubation) was assessed after up to 72 h exposure time (D). The asterisk marks the cell population that stains positive for phospho-histone H2A.X.

repair (Fig. 4C and D) [26,27]. Massive induction of γ-H2AX was observed in response to UVB-exposure serving as a positive control (Fig. 4C). In contrast, no significant upregulation of γ-H2AX was observed at 3 h of exposure to FAdo in MiaPaCa-2 (Fig. 4C) or A375 cells (data not shown) suggesting that FAdo-induced early DNA damage is not associated with double strand breaks. At 24 h FAdo exposure, a small increase in γ-H2AX-positive cells was detected (Fig. 4D). At 72 h FAdo exposure, pronounced staining for γ-H2AX was detected. This finding is consistent with massive DNA double strand cleavage during later stages of apoptosis that occurs upon prolonged FAdo exposure (Fig. 1B and D–G). Taken together, these data demonstrate for the first time that FAdo exposure is associated with significant induction of genotoxic stress observable in various cancer cell lines within 1 h of exposure and not associated with DNA double strand breaks.

3.5. *FAdo treatment induces early changes in stress-response gene expression*

After demonstrating anti-proliferative, apoptogenic, ATP-depleting, and genotoxic activity of FAdo against MiaPaCa-2, A375, and other cancer cell lines, modulation of stress response gene expression was examined in MiaPaCa-2 human pancreas carcinoma cells exposed to FAdo (Figs. 5 and 6, Table 2). First, the RT^2 Human Stress and Toxicity Pathway Finder™ PCR Expression Array technology (SuperArray, Frederick, MD, USA) was applied to MiaPaCa-2 cells exposed to FAdo (10 μM, 72 h exposure) to assess expression of 84 stress-related genes contained on the array (Fig. 5A). A summary of genes that were at least threefold up- or downregulated over untreated control cells is presented in Table 2. Expression of the four genes that displayed the most pronounced degree of FAdo-induced upregulation [CDKN1A (17.3-fold); DDIT3 (17.5-fold); GADD45A (17.1-fold); HMOX1 (19.8-fold)] was then confirmed using array-independent primer sets (Fig. 5B). A time course of FAdo-dependent induction of these genes was then established using quantitative RT-PCR (Fig. 5B). The DNA-damage response genes *DNA-damage-inducible transcript 3* (DDIT3) and *growth arrest and DNA-damage-inducible, alpha* (GADD45A) were strongly upregulated by at least 12-fold within 12 h of FAdo exposure, consistent with an early cellular response to FAdo-induced genotoxic stress as described above (Fig. 4) [28–31]. Moreover, expression of *heme oxygenase-1* (HMOX1) encoding the crucial antioxidant enzyme HO-1 known to be upregulated in response to metabolic and oxidative stress was significantly induced within 4 h of FAdo exposure and could also be detected by Western analysis after 24 and 72 h exposure (Fig. 6D) [32,33]. Most importantly, the cell cycle regulator and stress-respon-

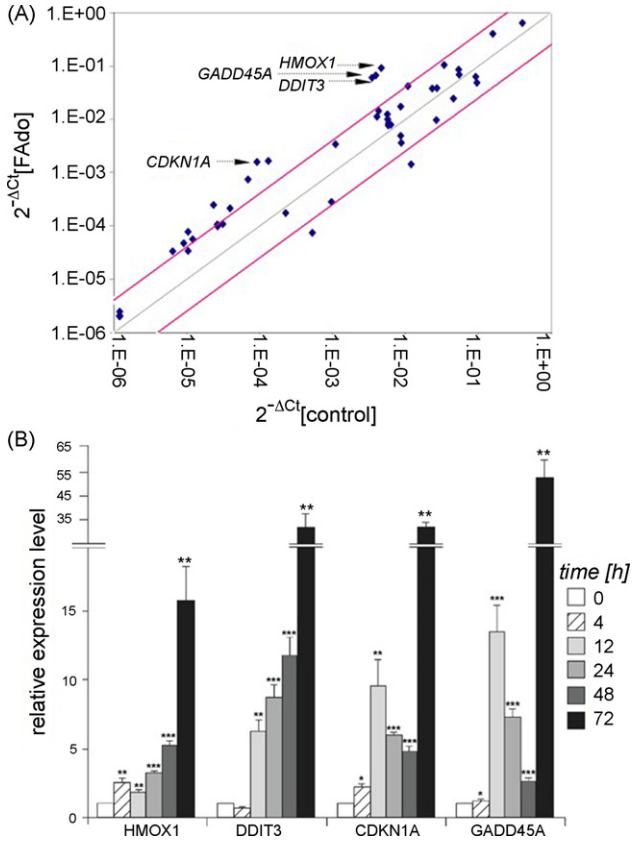

Fig. 5 – Early expression of CDKN1A and other stress response genes in MiaPaCa-2 and A375 cells exposed to FAdo. (A) Differential gene expression in MiaPaCa-2 cells exposed to FAdo (10 μM, 72 h) or left untreated was analyzed using the RT^2 Human Stress and Toxicity Pathway Finder™ PCR Expression Array performed in three independent repeat experiments. Changes in cycle threshold (Ct) for genes of interest relative to GAPDH for untreated control (*x*-axis) and FAdo-treated (*y*-axis) cells are displayed as scatter blot ($p < 0.05$). Upper and lower lines represent the cut-off indicating four fold up- or down-regulated expression, respectively. The arrows specify the four genes with the highest FAdo-induced upregulation of expression. (B) Time course analysis of FAdo target gene upregulation (10 μM FAdo, 4–72 h exposure) by quantitative RT-PCR using array-independent primer sets with normalization for GAPDH expression levels. Relative expression levels in response to mock treatment (control) and FAdo exposure were determined in three repeat experiments ($n = 3$, mean ± S.D.).

sive tumor suppressor gene *cyclin-dependent kinase inhibitor* 1A (CDKN1A) was significantly upregulated within 4 h, and 10-fold induction was observed at 12 h exposure to FAdo. Due to its crucial role in cell cycle regulation and anti-mitotic activity in response to cytotoxic stress [34], FAdo upregulation of cellular CDKN1A gene expression was then examined at the protein level by p21 immunoblot analysis in MiaPaCa-2 and A375 cells (Fig. 6). In MiaPaCa-2 (Fig. 6A–C) and A375 cells (Fig. 6E and F), FAdo treatment dose-dependently upregulated

Table 2 – Differential gene expression analysis of FAdo-treated MiaPaCa-2 cells.

Gene symbol	Fold change	*p*-Value
ANXA5 (NM_001154)	3.1	0.001
CCL3 (NM_002983)	7.5	0.019
CCL4 (NM_002984)	4.7	0.020
CDKN1A (NM_000389)	17.3	0.001
CRYAB (NW_001885)	5.5	0.025
CYP1A1 (NM_000499)	−7.0	0.002
CYP2E1 (NM_000773)	5.3	0.021
CYP7A1 (NW_000780)	3.7	0.038
DDIT3 (NM_004083)	17.5	0.001
DNAJB4 (NM_007034)	3.3	0.020
FASLG (NM_00639)	3.3	0.022
GADD45A (NU_001924)	17.1	0.001
GDF15 (NM_00864)	12.7	0.045
GPX1 (NM_000581)	−3.4	0.002
HWOX1 (NM_002133)	19.8	0.001
HSPA6 (NM_002155)	10.8	0.014
LTA (NM_000595)	10.7	0.008
MT5A (NM_005953)	3.1	0.027
PTGS1 (NM_000962)	5.2	0.009
SERPINE1 (NM_000602)	3.9	0.033
TNF (NM_000694)	3.5	0.030
UGT1A4 (NM_007120)	4.1	0.016

Changes in gene expression were detected by RT^2 Human Stress and Toxicity Pathway Finder™ PCR Expression Array analysis of MiaPaCa-2 cells exposed to FAdo or left untreated as detailed in Fig. 5A. Expression array analysis was performed in three independent repeats and analyzed using the two-sided Student's *t*-test. The table summarizes statistically significant expression changes by at least threefold ($p < 0.05$).

p21 protein levels. Again, 5′-AdA treatment (Fig. 6C and F) or ADK-siRNA intervention (Fig. 6E) suppressed FAdo-induced p21 upregulation. Remarkably, FAdo-induced upregulation of cellular p21 levels was apparent within 3 h of exposure in MiaPaCa-2 cells, consistent with a mechanistic involvement of p21 upregulation in FAdo-inhibition of proliferation and cell cycle progression (Fig. 6B).

In summary, these gene expression data suggest that in MiaPaCa-2 cells, FAdo treatment induces a rapid DNA damage response, massive upregulation of the tumor suppressor gene CDKN1A, and sustained expression of the stress response gene HMOX1. Similarly, FAdo-induced upregulation of CDKN1A expression could be observed in A375 cells and could be completely abolished by ADK-knockdown or ADK-enzymatic inhibition.

4. Discussion

Anti-proliferative and apoptogenic effects of the nucleoside FAdo against human cancer cells are well documented, but little is known about the molecular mechanisms that underlie FAdo-cytotoxicity. Earlier work suggests the involvement of the mitochondrial pathway of apoptosis with changes in redox and energy balance, mitochondrial transmembrane depolarization, cytochrome C release, and modulation of Bcl-2 family proteins in cytotoxicity induced by FAdo and other cytokinin nucleosides [3,6,12–14]. More recently, unbiased screening of a chemical library for inhibition of genes encoding cyclin D1

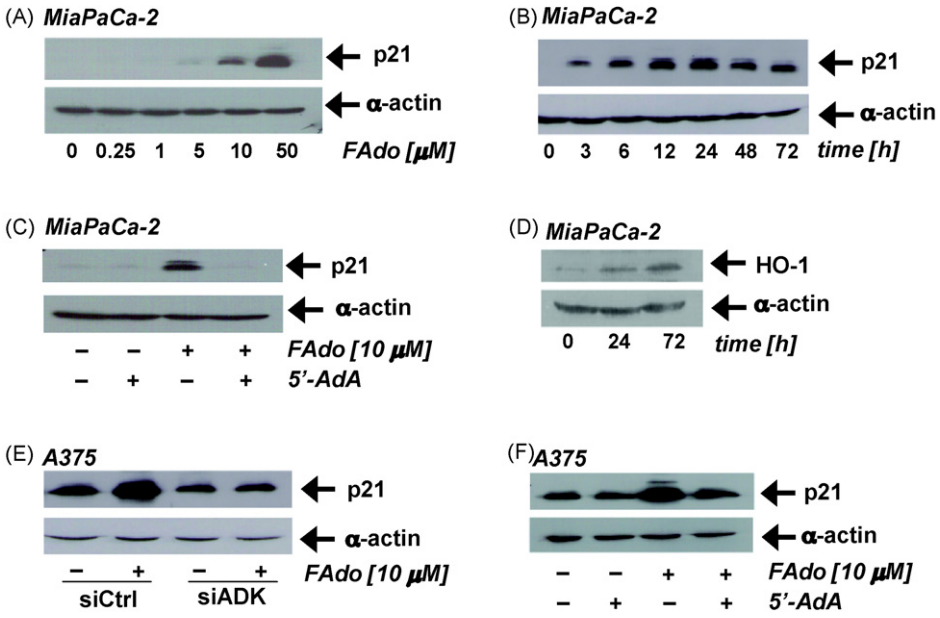

Fig. 6 – Early upregulation of p21 and HO-1 protein levels in MiaPaCa-2 and A375 cells exposed to FAdo. Western blot analysis of FAdo-induced p21 and HO-1 upregulation was performed in MiaPaCa-2 (panels A–D) and A375 cells (panels E–F). (A) Dose response of FAdo-induced p21 upregulation analyzed at 24 h exposure. (B) Time course of p21 upregulation induced by FAdo (10 μM). (C and F) Suppression of FAdo-induced p21 upregulation (10 μM FAdo, 24 h) by 5′-AdA (2 μM). (D) HO-1 upregulation by FAdo treatment (10 μM, 24 and 72 h exposure). (E) ADK-siRNA-mediated suppression of p21 upregulation (10 μM FAdo, 24 h).

(CCND1) and cyclin D2 (CCND2) has identified FAdo as a potent inhibitor of CCND2 trans-activation leading to downregulation of cyclins D1 and D2 within 16 h of FAdo exposure in human myeloma cell lines [14].

Our work demonstrates that ATP depletion, induction of DNA damage, and upregulation of CDKN1A at the mRNA and protein level are early consequences of FAdo exposure in MiaPaCa-2 cells, accompanied by upregulation of a stress and DNA damage response involving sustained expression of HMOX1, DDIT3, and GADD45. Importantly, our experiments demonstrate for the first time that FAdo rapidly impairs genomic integrity, observed in MiaPaCa-2 and A375 cells within 60 min of exposure using alkaline single cell electrophoresis (comet assay) (Fig. 4A and B). If performed under strongly alkaline lysis conditions (pH > 13), the comet assay reveals the presence of DNA double strand breaks, single strand breaks, alkali-labile sites and single strand breaks associated with incomplete excision repair sites [21,24,25]. As another independent marker of genotoxicity, phosphorylation of histone H2A.X at serine 139 (γ-H2A.X) occurs within minutes in response to DNA double strand breaks requiring the activation of the phosphatidylinositol-3-OH-kinase-like family of protein kinases including ATM and ATR [27]. However, formation of γ-H2A.X in response to FAdo exposure occurred with much delay and could only be detected at exposure times of at least 24 h (Fig. 4C and D). As a positive control, early induction of γ-H2A.X by UVB irradiation was used (Fig. 4C). UVB-induced γ-H2A.X has been shown to originate from DNA structures generated during the processing of UV-induced lesions leading to phosphorylation by the ATR kinase [26]. Therefore, early detection of comet formation (Fig. 4A and B) in the absence of H2A.X phosphorylation (Fig. 4C and D) in FAdo-exposed MiaPaCa-2 cells is most consistent with a mechanism of FAdo-genotoxicity that does not result in direct DNA strand breaks, but involves lesions that can be detected through the alkaline comet assay, i.e. alkylated DNA bases that form alkaline-labile sites. Earlier work has shown that chemical incorporation of FA-nucleotides into plasmid DNA induces DNA polymerase-dependent base misincorporation in an acellular replication assay [35]. FAdo-dependent early cellular DNA damage may therefore originate from ADK-dependent FAdo-nucleotide formation, followed by reductive metabolism into the corresponding FA-2′-deoxynucleotide, and subsequent misincorporation into DNA, a hypothesis to be tested by future experiments.

Consistent with a causative role of early DNA damage in the molecular mechanism of FAdo cytotoxicity, expression array analysis revealed rapid FAdo-induced upregulation of GADD45A and DDIT3 [also called GADD153 or C/EBP homologous protein (CHOP)], genes coordinatively upregulated after DNA damage [28–31]. Upregulation of these genes has been shown to induce growth arrest and apoptosis in response to serum starvation and genotoxic stress signals [36–40]. Furthermore, expression array (Fig. 5) and Western analysis (Fig. 6) performed on MiaPaCa-2 pancreas carcinoma and A375 melanoma cells demonstrated FAdo-induced upregulation of the cyclin-dependent kinase inhibitor and tumor suppressor gene CDKN1A within hours of FAdo exposure. The CDKN1A-encoded protein p21 is a member of the Cip/Kip family of cyclin-dependent kinase inhibitors known to be upregulated in response to DNA damage and oxidative stress, and p21 plays an essential role in growth arrest after DNA damage by

binding and inhibiting cyclin/Cdk complexes [34,41]. As a major cellular proliferation inhibitor that synergizes with other tumor suppressors, p21 has been associated with induction of cell cycle arrest in G1 as well as G2/M-phase and may therefore be an important mediator of FAdo-induced cell cycle alterations and anticancer activity [42,43]. p21 expression in response to DNA damage and other cellular stress has been shown to be regulated largely at the transcriptional level by both p53-dependent and -independent mechanisms including DDIT3 (GADD153)-mediated pathways [34,39]. Taken together, our expression analysis strongly suggests that FAdo-induced cytotoxicity may therefore be mediated through upregulation of GADD45A, DDIT3, and CDKN1A resulting in inhibition of cell proliferation and induction of apoptosis after early induction of energy crisis and DNA damage.

Our work demonstrates that in addition to early induction of DNA damage, cellular ATP depletion occurs rapidly as a consequence of FAdo exposure in all cancer cell lines and primary human skin cells examined (Fig. 3). Involvement of ADK in FAdo-induced ATP depletion was validated by pharmacological (5′-AdA) and genetic (siRNA) target modulation (Fig. 3). Earlier work has observed cytokinin riboside-induced (N^6-isopentenyladenosine and FAdo) ATP depletion in human HL60 leukemia cells [3,6]. An established molecular pathway that may link energy crisis and DNA damage in response to potent alkylating agents is DNA damage-induced poly(ADP-ribose) polymerase (PARP) activation, leading rapidly to cellular NAD-depletion and breakdown of mitochondrial ATP production [44,45]. However, in our experiments FAdo-induced cellular energy crisis could not be blocked by performing FAdo exposure in the presence of PARP inhibitors including 3-aminobenzamide, a standard intervention that protects against PARP-mediated energy crisis induced by many DNA alkylating agents [44]. Moreover, no depletion of the cellular NAD-pool, an early consequence of PARP activation, was observed during the course of 6 h FAdo exposure of cells, again disqualifying an involvement of PARP activation in FAdo-induced ATP depletion (data not shown). In addition, the absence of DNA double strand breaks as assessed by γ-H2A.X-staining until 24 h FAdo exposure is inconsistent with PARP-mediated energy crisis as a consequence of DNA damage.

The mechanism of ATP depletion by FAdo observed in all human cancer cell lines and primary skin cells tested by us is currently unknown. Future experiments will address the hypothesis that FAdo, after ADK-dependent phosphorylation and activation, interferes with ATP synthesis and metabolism in analogy to other ADK-dependent ATP-depleting adenosine-derivatives such as 2-chloro- and 8-chloroadenosine [46,47]. 8-Chloroadenosine, currently in phase I clinical studies for anticancer intervention (clinicaltrials.gov identifier NCT00714103), rapidly depletes cellular ATP levels through structure-based inhibition of mitochondrial ATP synthase by the 8-chloroadenosine nucleotide metabolite. Our future experiments will aim at elucidating the molecular mechanism of ATP depletion and its mechanistic relationship with FAdo-induced genotoxic stress as observed in MiaPaCa-2 carcinoma and A375 melanoma cells.

Remarkably, our experiments indicate that the pronounced anti-proliferative effects of FAdo are not specific for cancer cells. Proliferation of primary human keratinocytes and fibroblasts was completely inhibited by submicromolar concentrations of FAdo (Table 1), and rapid depletion of cellular ATP was observed in primary cells exposed to low micromolar concentrations of FAdo (Fig. 3A). It is important to note that the lack of cancer cell selectivity as observed in our cell culture based studies does not preclude anticancer efficacy of FAdo that has been documented in recent murine xenograft studies. Indeed, ADK-dependence of FAdo-induced ATP depletion and cytotoxicity suggests that cancer-cell selectivity may be achieved based on the known overexpression of ADK by tumor tissue as recently documented in human colorectal cancer [48]. Interestingly, the nucleoside triciribine, another ADK-activated prodrug, has recently been proposed as a chemotherapeutic agent for personalized anticancer therapy based on ADK expression profiling [49]. Moreover, an increased susceptibility of rapidly proliferating cells for energy depletion combined with the compromised ability of cancer cells for mitochondrial energy production have been suggested as a potential functional target for anticancer intervention [47,50,51], and it is therefore possible that FAdo-induced energy crisis preferentially impairs tumor cell performance.

Acknowledgements

Supported in part by grants from the National Institutes of Health [R01CA122484, ES007091, ES06694, Arizona Cancer Center Support Grant CA023074], the Arizona Biomedical Research Commission (ABRC 0721), NSF (DGE-0114420 to CMC), and the Arizona Science Foundation (to SL).

REFERENCES

[1] Vesely J, Havlicek L, Strnad M, Blow JJ, Donella-Deana A, Pinna L, et al. Inhibition of cyclin-dependent kinases by purine analogues. Eur J Biochem 1994;224:771–86.
[2] Havlicek L, Hanus J, Vesely J, Leclerc S, Meijer L, Shaw G, et al. Cytokinin-derived cyclin-dependent kinase inhibitors: synthesis and cdc2 inhibitory activity of olomoucine and related compounds. J Med Chem 1997;40:408–12.
[3] Ishii Y, Hori Y, Sakai S, Honma Y. Control of differentiation and apoptosis of human myeloid leukemia cells by cytokinins and cytokinin nucleosides, plant redifferentiation-inducing hormones. Cell Growth Differ 2002;13:19–26.
[4] Skoog F. Cytokinins in regulation of plant growth. Basic Life Sci 1973;2:147–84.
[5] Vermeulen K, Strnad M, Havlicek L, Van Onckelen H, Lenjou M, Nijs G, et al. Plant cytokinin analogues with inhibitory activity on cyclin-dependent kinases exert their antiproliferative effect through induction of apoptosis initiated by the mitochondrial pathway: determination by a multiparametric flow cytometric analysis. Exp Hematol 2002;30:1107–14.
[6] Mlejnek P, Dolezel P. Apoptosis induced by N6-substituted derivatives of adenosine is related to intracellular accumulation of corresponding mononucleotides in HL-60 cells. Toxicol In Vitro 2005;19:985–90.
[7] Miller CO, Skoog F, Von Saltza MH, Strong M. Kinetin, a cell division factor from deoxyribonucleic acid. J Am Chem Soc 1995;77:1329–34.

[8] Wondrak GT, Tressl R, Rewicki D. Maillard reaction of free and nucleic acid-bound 2-deoxy-D-ribose and D-ribose with omega-amino acids. J Agric Food Chem 1997;45:321–7.
[9] Olsen A, Siboska GE, Clark BF, Rattan SI. N(6)-furfuryladenine, kinetin, protects against Fenton reaction-mediated oxidative damage to DNA. Biochem Biophys Res Commun 1999;265:499–502.
[10] Rattan SI, Clark BF. Kinetin delays the onset of ageing characteristics in human fibroblasts. Biochem Biophys Res Commun 1994;201:665–72.
[11] Slaugenhaupt SA, Mull J, Leyne M, Cuajungco MP, Gill SP, Hims MM, et al. Rescue of a human mRNA splicing defect by the plant cytokinin kinetin. Hum Mol Genet 2004;13:429–36.
[12] Griffaut B, Bos R, Maurizis JC, Madelmont JC, Ledoigt G. Cytotoxic effects of kinetin riboside on mouse, human and plant tumour cells. Int J Biol Macromol 2004;34:271–5.
[13] Choi BH, Kim W, Wang QC, Kim DC, Tan SN, Yong JW, et al. Kinetin riboside preferentially induces apoptosis by modulating Bcl-2 family proteins and caspase-3 in cancer cells. Cancer Lett 2008;261:37–45.
[14] Tiedemann RE, Mao X, Shi CX, Zhu YX, Palmer SE, Sebag M, et al. Identification of kinetin riboside as a repressor of CCND1 and CCND2 with preclinical antimyeloma activity. J Clin Invest 2008;118:1750–64.
[15] Pfaffl MW. A new mathematical model for relative quantification in real-time RT-PCR. Nucleic Acids Res 2001;29:e45.
[16] Pfaffl MW, Horgan GW, Dempfle L. Relative expression software tool (REST) for group-wise comparison and statistical analysis of relative expression results in real-time PCR. Nucleic Acids Res 2002;30:e36.
[17] Wondrak GT, Cabello CM, Villeneuve NF, Zhang S, Ley S, Li Y, et al. Cinnamoyl-based Nrf2-activators targeting human skin cell photo-oxidative stress. Free Radic Biol Med 2008;45:385–95.
[18] Wondrak GT, Roberts MJ, Jacobson MK, Jacobson EL. 3-Hydroxypyridine chromophores are endogenous sensitizers of photooxidative stress in human skin cells. J Biol Chem 2004;279:30009–20.
[19] Wondrak GT, Jacobson MK, Jacobson EL. Antimelanoma activity of apoptogenic carbonyl scavengers. J Pharmacol Exp Ther 2006;316:805–14.
[20] Wondrak GT. NQO1-activated phenothiazinium redox cyclers for the targeted bioreductive induction of cancer cell apoptosis. Free Radic Biol Med 2007;43:178–90.
[21] Roberts MJ, Wondrak GT, Cervantes-Laurean D, Jacobson MK, Jacobson EL. DNA damage by carbonyl stress in human skin cells. Mutat Res 2003;522:45–56.
[22] Dong Z, Bode AM. The role of histone H3 phosphorylation (Ser10 and Ser28) in cell growth and cell transformation. Mol Carcinog 2006;45:416–21.
[23] Camici M, Turriani M, Tozzi MG, Turchi G, Cos J, Alemany C, et al. Purine enzyme profile in human colon-carcinoma cell lines and differential sensitivity to deoxycoformycin and 2′-deoxyadenosine in combination. Int J Cancer 1995;62:176–83.
[24] Singh NP, McCoy MT, Tice RR, Schneider EL. A simple technique for quantitation of low levels of DNA damage in individual cells. Exp Cell Res 1988;175:184–91.
[25] Tice RR, Agurell E, Anderson D, Burlinson B, Hartmann A, Kobayashi H, et al. Single cell gel/comet assay: guidelines for in vitro and in vivo genetic toxicology testing. Environ Mol Mutagen 2000;35:206–21.
[26] Hanasoge S, Ljungman M. H2AX phosphorylation after UV irradiation is triggered by DNA repair intermediates and is mediated by the ATR kinase. Carcinogenesis 2007;28:2298–304.
[27] Kinner A, Wu W, Staudt C, Iliakis G. [gamma]-H2AX in recognition and signaling of DNA double-strand breaks in the context of chromatin. Nucleic Acids Res 2008;36:5678–94.
[28] Hollander MC, Sheikh MS, Bulavin DV, Lundgren K, Augeri-Henmueller L, Shehee R, et al. Genomic instability in Gadd45a-deficient mice. Nat Genet 1999;23:176–84.
[29] Hildesheim J, Bulavin DV, Anver MR, Alvord WG, Hollander MC, Vardanian L, et al. Gadd45a protects against UV irradiation-induced skin tumors, and promotes apoptosis and stress signaling via MAPK and p53. Cancer Res 2002;62:7305–15.
[30] Hildesheim J, Fornace Jr AJ. Gadd45a: an elusive yet attractive candidate gene in pancreatic cancer. Clin Cancer Res 2002;8:2475–9.
[31] Barsyte-Lovejoy D, Mao DY, Penn LZ. c-Myc represses the proximal promoters of GADD45a and GADD153 by a post-RNA polymerase II recruitment mechanism. Oncogene 2004;23:3481–6.
[32] Cabello CM, Bair III WB, Wondrak GT. Experimental therapeutics targeting the redox Achilles heel of cancer. Curr Opin Investig Drugs 2007;8:1022–37.
[33] Wang XJ, Sun Z, Villeneuve NF, Zhang S, Zhao F, Li Y, et al. Nrf2 enhances resistance of cancer cells to chemotherapeutic drugs, the dark side of Nrf2. Carcinogenesis 2008;29:1235–43.
[34] Gartel AL, Tyner AL. The role of the cyclin-dependent kinase inhibitor p21 in apoptosis. Mol Cancer Ther 2002;1:639–49.
[35] Wyszko E, Barciszewska MZ, Markiewicz M, Szymanski M, Markiewicz WT, Clark BF, et al. ''Action-at-a-distance'' of a new DNA oxidative damage product 6-furfuryl-adenine (kinetin) on template properties of modified DNA. Biochim Biophys Acta 2003;1625:239–45.
[36] Sarkar D, Su ZZ, Lebedeva IV, Sauane M, Gopalkrishnan RV, Valerie K, et al. mda-7 (IL-24) mediates selective apoptosis in human melanoma cells by inducing the coordinated overexpression of the GADD family of genes by means of p38 MAPK. Proc Natl Acad Sci USA 2002;99:10054–9.
[37] Scott DW, Loo G. Curcumin-induced GADD153 gene up-regulation in human colon cancer cells. Carcinogenesis 2004;25:2155–64.
[38] Gao H, Jin S, Song Y, Fu M, Wang M, Liu Z, et al. B23 regulates GADD45a nuclear translocation and contributes to GADD45a-induced cell cycle G2–M arrest. J Biol Chem 2005;280:10988–96.
[39] Zu K, Bihani T, Lin A, Park YM, Mori K, Ip C. Enhanced selenium effect on growth arrest by BiP/GRP78 knockdown in p53-null human prostate cancer cells. Oncogene 2006;25:546–54.
[40] Shao S, Wang Y, Jin S, Song Y, Wang X, Fan W, et al. Gadd45a interacts with aurora-A and inhibits its kinase activity. J Biol Chem 2006;281:28943–50.
[41] Weiss RH. p21Waf1/Cip1 as a therapeutic target in breast and other cancers. Cancer Cell 2003;4:425–9.
[42] Niculescu III AB, Chen X, Smeets M, Hengst L, Prives C, Reed SI. Effects of p21(Cip1/Waf1) at both the G1/S and the G2/M cell cycle transitions: pRb is a critical determinant in blocking DNA replication and in preventing endoreduplication. Mol Cell Biol 1998;18:629–43.
[43] Shangary S, Ding K, Qiu S, Nikolovska-Coleska Z, Bauer JA, Liu M, et al. Reactivation of p53 by a specific MDM2 antagonist (MI-43) leads to p21-mediated cell cycle arrest and selective cell death in colon cancer. Mol Cancer Ther 2008;7:1533–42.
[44] Pogrebniak A, Schemainda I, Pelka-Fleischer R, Nussler V, Hasmann M. Poly ADP-ribose polymerase (PARP) inhibitors transiently protect leukemia cells from alkylating agent induced cell death by three different effects. Eur J Med Res 2003;8:438–50.

[45] Zong WX, Ditsworth D, Bauer DE, Wang ZQ, Thompson CB. Alkylating DNA damage stimulates a regulated form of necrotic cell death. Genes Dev 2004;18:1272–82.
[46] Chen LS, Zhang S, Nowak BJ, Ayres M, Stellrecht CM, Krett NL, et al. Inhibition of ATP synthase by a halogenated adenosine analog. In: Proceedings of the 99th Annual Meeting of the American Association for Cancer Research. San Diego, CA/Philadelphia (PA): AACR; 2008. Abstract nr 3182.
[47] Bastin-Coyette L, Smal C, Cardoen S, Saussoy P, Van den Neste E, Bontemps F. Mechanisms of cell death induced by 2-chloroadenosine in leukemic B-cells. Biochem Pharmacol 2008;75:1451–60.
[48] Giglioni S, Leoncini R, Aceto E, Chessa A, Civitelli S, Bernini A, et al. Adenosine kinase gene expression in human colorectal cancer. Nucleosides Nucleotides Nucleic Acids 2008;27:750–4.
[49] Shedden K, Townsend LB, Drach JC, Rosania GR. A rational approach to personalized anticancer therapy: chemoinformatic analysis reveals mechanistic gene–drug associations. Pharm Res 2003;20:843–7.
[50] Goldin N, Heyfets A, Reischer D, Flescher E. Mitochondria-mediated ATP depletion by anti-cancer agents of the jasmonate family. J Bioenerg Biomembr 2007;39:51–7.
[51] Shaw RJ. Glucose metabolism and cancer. Curr Opin Cell Biol 2006;18:598–608.